

Study of the Temperature Dependence of the Reaction of NO_3 with CH_3I and the Estimation of Its Impact on Atmospheric Iodine Chemistry

Yukio Nakano,*[1] Hiromi Ukeguchi,[1] Takashi Ishiwata,[1] Yugo Kanaya,[2] Hiroto Tachikawa,[3] Atsushi Ikeda,[4] Shigeyoshi Sakaki,[4] and Masahiro Kawasaki[5]

[1]Graduate School of Information Sciences, Hiroshima City University, Hiroshima 731-3194

[2]Frontier Research Center for Global Change, Japan Agency for Marine-Earth Science and Technology, Yokohama 236-0001

[3]Graduate School of Engineering, Hokkaido University, Sapporo 060-8628

[4]Division of Molecular Theory for Science and Technology, Department of Molecular Engineering, Kyoto University, Kyoto 615-8510

[5]Division of Photochemical Reaction, Department of Molecular Engineering, Kyoto University, Kyoto 615-8510

Received December 3, 2007; E-mail: yukio_n@hiroshima-cu.ac.jp

The rate constants of the reaction of NO_3 with CH_3I, which can affect iodine chemistry in the atmosphere, were measured in the temperature range of 298–323 K with cavity ring-down spectroscopy. The reaction has a rate constant of $k = (4.1 \pm 0.2) \times 10^{-13}$ cm^3 molecule^{-1} s^{-1} at 298 K. Uncertainties reported herein are one standard deviation. On the basis of an Arrhenius plot in the region of 298–323 K, the reaction has an activation energy ($E_a = 13 \pm 3$ kJ mol^{-1}). Density functional and coupled-cluster calculations suggest that the reaction proceeds via a transition state in which the hydrogen atom is nearly located at the middle position between the carbon atom of CH_3I and the oxygen atom of NO_3 to give $HNO_3 + CH_2I$. On the atmospheric implications, box model simulations indicate that the present reaction has an important effect on the levels and diurnal patterns of the mixing ratios of NO_3 and CH_3I, and also on the activation of iodine chemistry in the atmosphere.

Nitrogen trioxide, i.e., nitrate radical NO_3, is considered to be one of the most important oxidizers especially in urban areas, because NO_3 is formed by the reaction of O_3 with NO_2 included in automobile exhaust emissions. Solar photolysis suppresses the concentration of NO_3 in the daytime resulting in the mixing ratio of NO_3 peaking at nighttime. Saiz-Lopez and Plane have recently reported the observations of a significant nighttime concentration (averaging 7 pptv) of NO_3 with the use of differential optical absorption spectroscopy over the marine boundary layer at the Mace Head Atmospheric Research Station on the west coast of Ireland during August 2002.[1]

Alkyl iodides are produced by various types of macroalgae and phytoplankton in the ocean and emitted into the atmosphere. Sunlight photolysis and the sequential reactions of alkyl iodides generate iodine monoxide radical (IO) which is considered to be important in the atmosphere because IO affects the oxidizing capacity of the atmosphere by being involved in the ozone depleting cycle as an efficient oxidizer.[2–6] Recent studies have also suggested the importance of IO for aerosol formation in the atmosphere. O'Dowd et al. reported a new aerosol particle formation pathway from condensable iodine-containing vapors via IO radicals.[7] They demonstrated by using an aerosol formation model that concentrations of condensable iodine-containing vapors over the open ocean were sufficient to influence marine particle formation.[8] Consequently they suggested that emission of iodine-containing compounds from marine environments had a potentially significant effect on global radiative forcing. If this phenomenon occurs on a large scale, it could have significant effects on climate.[9]

At nighttime, IO has been considered to be absent in the marine boundary layer, because it was considered to be mainly formed from the sunlight photolysis of alkyl iodides. However, Saiz-Lopez and Plane[1] have observed a significant nighttime concentration (up to 7 pptv) of IO as well as NO_3 at the Mace Head Atmospheric Research Station. They attributed the high concentration of IO in the night to an $I_2 + NO_3$ reaction.

In our previous study, we measured the rate constants of the reaction of $NO_3 + CH_3I$ with cavity ring-down spectroscopy in 20–200 Torr of N_2 diluent at 298 K.[10]

$$NO_3 + CH_3I \rightarrow HNO_3 + CH_2I \quad (1)$$

The rate constant for the reaction of $NO_3 + CH_3I$ was determined to be $(4.1 \pm 0.2) \times 10^{-13}$ cm^3 molecule^{-1} s^{-1} in 100 Torr of N_2 diluent at 298 K and was pressure-independent. These results indicated that the $NO_3 + CH_3I$ reaction would play an important role in loss of CH_3I during the nighttime and might act as a new source of IO in the atmosphere by combining sequential reactions.

In this study, we measured the rate constants of the $NO_3 + CH_3I$ reaction at several temperatures to determine an Arrhenius expression that is indispensable for atmospheric

Published on the web August 11, 2008; doi:10.1246/bcsj.81.938

modeling. In our previous study, we determined the rate constant of $NO_3 + CH_3I$ at 298 K by using IBM Chemical Kinetics Simulator Program to take account of some side reactions. Unfortunately, by the lack of knowledge of the temperature dependence of these reactions used in simulation, we could not explore the temperature dependence of the rate constant for the reaction of $NO_3 + CH_3I$. In this study, the measurements were achieved by reducing the concentration of NO_3 by a factor of ten compared to that in our previous study. Under these conditions, the influence of side reactions was suppressed and the rate constant of the reaction of $NO_3 + CH_3I$ at several temperatures could be determined without knowledge of the temperature dependence of some side reactions shown in the results section. The density functional theory (DFT) calculations were carried out to investigate the reaction pathway. Finally, to investigate the impact of the $NO_3 + CH_3I$ reaction on the atmospheric chemistry, simulations were performed using a zero-dimensional box model.

Experimental

Our cavity ring-down spectroscopy apparatus is similar to one previously reported.[11,12] Two pulsed lasers were employed in the experiments. A pulsed Nd^{3+}:YAG laser (Continuum, Surelite II, 0.5–2 mJ cm^{-2} pulse^{-1}) was used to photolyze dinitrogen pentaoxide (N_2O_5) at 266 nm to generate NO_3 radicals. A dye laser (Sirah, Cobra-Stretch; DCM Dye) pumped by the 532 nm output of another pulsed Nd^{3+}:YAG laser was used to measure the concentration of NO_3. After the photolysis laser beam traversed a reaction cell nearly collinear to the axis of the ring-down cavity, the probe laser beam was injected through one of two high-reflectivity mirrors which made up the ring-down cavity. The ring-down time was used to measure the NO_3 concentration. As a function of the delay time between the photolysis and probe laser pulses, the decay of the light intensity was recorded using a digital oscilloscope (Tektronix TDS430A) and transferred to a personal computer. The ring-down decay of the probe light intensity is given by equation,

$$I(t) = I_0 \exp(-t/\tau) = I_0 \exp(-t/\tau_0 - \sigma nc(L_R/L)t) \quad (2)$$

where $I(t)$ is the intensity of light at time t. τ_0 is the empty cavity ring-down time (5.6 μs at 662.0 nm). L_R is the length of the reaction region (0.46 m) while L is the cavity length (1.04 m); τ is the measured cavity ring-down time; n and σ are the concentration and absorption cross section of the species of interest; and c is the speed of light.

The electronic transition NO_3 ($B^2E' \leftarrow X^2A'_2$) was monitored at 662.0 nm. The absorption of NO_3 was converted to concentration by using the reported absorption cross section at 662.0 nm, $\sigma_{NO_3} = 2.25 \times 10^{-17}$ cm^2 molecule^{-1}.[13–15]

The reaction cell consisting of a Pyrex glass tube (21 mm i.d.) was evacuated by an oil rotary pump with liquid N_2 trap. The volume of the detection region of the reaction cell was 160 cm^3. The total flow rate was kept constant at 1.0×10^3 cm^3 min^{-1} (STP). Experiments were performed with 1 Hz laser operation. Hence, the gas mixture in the detection region was refreshed in 1–2 laser shots under the present pressure conditions. The temperature of the gas flow region was controlled within 1 K over the range from 298 to 323 K by circulation of thermostated water.

N_2O_5 was synthesized by the method reported by Caesar and Goldfrank.[16] CH_3I (99.5%) was subjected to repeated freeze–pump–thaw cycles before use. N_2 (>99.9995%) and O_2 (>99.995%) were used without further purification. The mixtures of N_2O_5/N_2 and CH_3I/N_2, prepared and stored in a glass bulb, were injected into the reaction cell using mass flow controllers. The concentrations of N_2O_5 and CH_3I in the reaction cell could be calculated by using the flow rates.

Computation

Geometries were fully optimized with the density functional theory (DFT) method under C_1 symmetry, where B3LYP functional was used for the exchange-correlation term.[17,18] We ascertained that each equilibrium geometry does not have imaginary frequencies and the transition state has one imaginary frequency. Energy changes were calculated by both the B3LYP and CCSD(T) methods. The cc-pVTZ basis sets[19] were employed for carbon, hydrogen, and oxygen. For iodine atom, the SDB-cc-pVTZ basis set was used for valence electrons and the Stuttgart–Dresden–Bonn relativistic effective core potentials were used to replace core electrons.[20] All theoretical calculations were carried out using the Gaussian 03 Revision C.02 program packages.[21]

Results

NO_3 radicals were produced by the 266 nm photolysis of N_2O_5 in 100 Torr of N_2.

$$N_2O_5 + h\nu(266\,\text{nm}) \rightarrow NO_3 + NO_2 \quad (3a)$$

$$\rightarrow NO_3 + NO + O(^3P) \quad (3b)$$

The branching ratios of reactions 3a and 3b were reported to be 0.62 and 0.38, respectively.[22,23] Figure 1 shows a typical decay profile of NO_3 in the absence of CH_3I at 298 K. Under these conditions, NO_3 possibly decays via the following pathways.

$$NO_3 \rightarrow \text{first-order loss (diffusion, wall loss, etc.)} \quad (4)$$

$$NO_3 + NO_3 \rightarrow \text{products} \quad (5)$$

The rate constant of reaction 5 was reported to be 2.3×10^{-16} cm^3 molecule^{-1} s^{-1} at 298 K.[13,24] NO_2, NO, and $O(^3P)$ possibly react with NO_3 via reactions 6–11 in Table 1.[13,23] The measured decay profiles of NO_3 were well reproduced

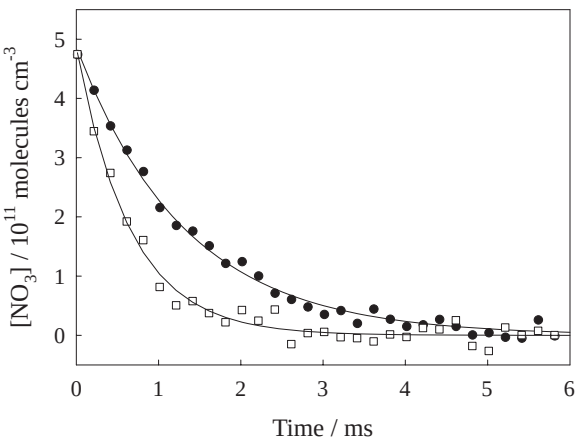

Figure 1. Typical decay profiles of NO_3 with and without CH_3I in 100 Torr of N_2 and O_2 diluent ($N_2/O_2 = 9/1$) at 298 K. $[CH_3I]_0 = 0$ (closed circles) and 1.3×10^{15} molecules cm^{-3} (open squares). The solid curves are a fit of eq 12 to the data.

Table 1. Reactions and Its Rate Constants Used in Our Kinetic Simulation for $NO_3 + CH_3I$ at 298 K in 100 Torr of N_2 Diluent

	Reaction	Rate constant/cm^3 molecule^{-1} s^{-1}	Ref.
(1)	$NO_3 + CH_3I \rightarrow HNO_3 + CH_2I$	$(4.2 \pm 0.3) \times 10^{-13}$	This work
(4)	$NO_3 \rightarrow$ first-order loss	Determined under each conditions	This work
(5)	$NO_3 + NO_3 \rightarrow$ products	2.3×10^{-16}	13, 24
(6a)	$NO_3 + NO_2 \rightarrow NO + NO_2 + O_2$	6.6×10^{-16}	13
(6b)	$NO_3 + NO_2 + M \rightarrow N_2O_5 + M$	8.8×10^{-13} a)	13
(7)	$NO_3 + NO \rightarrow NO_2 + NO_2$	2.7×10^{-11}	23
(8)	$NO_3 + O(^3P) \rightarrow NO_2 + O_2$	1.0×10^{-11}	13
(9)	$NO_2 + O(^3P) + M \rightarrow NO_3 + M$	8.2×10^{-13} a)	13
(10)	$NO_2 + O(^3P) \rightarrow NO + O_2$	1.1×10^{-11}	13
(11)	$NO + O(^3P) + M \rightarrow NO_2 + M$	2.6×10^{-13} a)	13
(15)	$NO_3 + CH_3 \rightarrow$ products	$(3.5 \pm 1.0) \times 10^{-11}$	25
(16)	$NO_3 + I \rightarrow NO_2 + IO$	$(1.0 \pm 0.3) \times 10^{-10}$	27
(18)	$CH_3 + I + M \rightarrow CH_3I + M$	$(9.96 \pm 4.98) \times 10^{-12}$ a)	28
(19)	$CH_3 + NO_2 \rightarrow$ products	$(3.26 \pm 0.40) \times 10^{-11}$	29
(20)	$I + I + M \rightarrow I_2 + M$	3.2×10^{-14}	30
(21)	$I + NO_2 + M \rightarrow INO_2 + M$	8.5×10^{-13} a)	23
(22a)	$CH_3I + O(^3P) \rightarrow CH_3 + IO$	1.8×10^{-11} b)	31
(22b)	$\rightarrow CH_2I + OH$		
(22c)	$\rightarrow H + I + CH_2O$		
(22d)	$\rightarrow I + CH_3O$		
(22e)	$\rightarrow HI + CH_2O$		
(22f)	$\rightarrow$ others		
(23)	$NO_3 + OH \rightarrow HO_2 + NO_2$	2.0×10^{-11}	13

a) In 100 Torr of N_2 diluents. b) Total rate constant. The yields for reaction pathways 22a–22e are 0.44, 0.16, 0.07, <0.03, and <0.05, respectively.

by single-exponential decay curves which are expressed by eq 12.[10,12]

$$[NO_3]_t = [NO_3]_0 \exp(-k't) \quad (12)$$

where $[NO_3]_t$ and $[NO_3]_0$ are the concentrations of NO_3 at time $t = t$ and 0, respectively. k' is the first-order rate constant for the loss of NO_3. These results indicate the influence of reactions 5–11 on the loss of NO_3 could be negligible, and the consumption of NO_3 was dominated by first-order loss (diffusion, wall loss, etc.) of reaction 4. Because the concentration of NO_3 was reduced to $\leqq 4.8 \times 10^{11}$ molecules cm^{-3}, the influence of reactions 5–11 were unimportant. The experimental conditions in our previous work and this work are summarized in Table 2. As shown in Figure 1, the decay profile of NO_3 in the absence of CH_3I was well reproduced by eq 12.

To determine the rate constant for $NO_3 + CH_3I$, the temporal profiles of $[NO_3]$ via the following processes were measured in the presence of large excess CH_3I, $(3.2–6.4) \times 10^{14}$ molecules cm^{-3} in 100 Torr of N_2 diluent. Under these conditions, the photodissociation of CH_3I at 266 nm induced CH_3 radicals and I atoms.

$$CH_3I + h\nu(266\,\text{nm}) \rightarrow CH_3 + I \quad (13)$$

The concentrations of CH_3 radicals and I atoms could be estimated from the photoabsorption cross sections at 266 nm.

$$[CH_3]_0 = [I]_0 = [NO_3]_0 \frac{\sigma_{CH_3I}[CH_3I]}{\sigma_{N_2O_5}[N_2O_5]} \quad (14)$$

σ_{CH_3I} and $\sigma_{N_2O_5}$ are 1.0×10^{-18} and 2.0×10^{-19} cm^2 molecule^{-1}, respectively.[13] Using eq 14, $[CH_3]_0$ and $[I]_0$ were estimated to be $(1.6–6.3) \times 10^{11}$ molecules cm^{-3}. CH_3 and I possibly react with NO_3 via reactions 15 and 16.

$$NO_3 + CH_3 \rightarrow \text{products} \quad (15)$$

$$NO_3 + I \rightarrow NO_2 + IO \quad (16)$$

The reported rate constant for reaction 15 is $k_{15} = (3.5 \pm 1.0) \times 10^{-11}$ cm^3 molecule^{-1} s^{-1} at 298 K and 100 Torr.[25] Chambers et al. reported the rate constant for reaction 16, $k_{16} = (4.5 \pm 1.9) \times 10^{-10}$ cm^3 molecule^{-1} s^{-1}.[26] In our previous study,[10] we could not reproduce the measured NO_3 decay profile with the simulation by the IBM Chemical Kinetics Simulator including the rate constant of $NO_3 + I$ reported by Chambers et al. NO_3 decay profile simulated with their value became much faster than that experimentally obtained even though the reaction $NO_3 + CH_3I$ was excluded from the simulation. And no recommended value is available for the rate constant of reaction 16 in the databases by NASA/JPL and IUPAC.[13,23] Therefore, in previous study, we adopted the reported rate constant of $NO_3 + Br$ ($k = 1.6 \times 10^{-11}$ cm^3 molecule^{-1} s^{-1}) for reaction 16. The value of the rate constant for reaction 16 was newly reported to be $k_{16} = (1.0 \pm 0.3) \times 10^{-10}$ cm^3 molecule^{-1} s^{-1} by Dillon et al. in 2008.[27] In this work, we adopted the rate constant of reaction 16 reported by Dillon et al. for the estimation of the influence of I atoms on the loss of NO_3 via reaction 16 and our kinetic simulations.

Briefly, we can estimate the influence of CH_3 radicals and I atoms on the loss of NO_3 via reactions 15 and 16. By taking products of estimated maximum concentrations of CH_3 radicals and I atoms ($[CH_3]_0 = [I]_0 = 6.3 \times 10^{11}$ molecules cm^{-3})

Table 2. Experimental Conditions[a] and the Rate Constants Obtained for $NO_3 + CH_3I$

No.	$[N_2O_5]_0$ /molecules cm^{-3}	$[CH_3I]_0$ /molecules cm^{-3}	$[O_2]_0$ /molecules cm^{-3}	Laser power /mJ cm^{-2} pules^{-1}	$[NO_3]_0$ /molecules cm^{-3}	$[I]_0$ and $[CH_3]_0$ /molecules cm^{-3}	k_1 /cm^3 molecule^{-1} s^{-1}	Ref.
1	1.3×10^{15}	$(0.3–3.2) \times 10^{15}$	0	10–15	$3–5 \times 10^{12}$	$(0.5–5) \times 10^{13}$	$(4.1 \pm 0.2) \times 10^{-13}$	10
2	3.0×10^{15}	$(0.1–1.3) \times 10^{15}$	3.2×10^{18}	3–6	$2–4 \times 10^{12}$	$(1.2–9.0) \times 10^{12}$	$(4.3 \pm 0.3) \times 10^{-13}$	10
3	1.3×10^{15}	$(3.2–6.4) \times 10^{14}$	0	0.5–2	$(1.3–3.6) \times 10^{11}$	$(1.6–6.3) \times 10^{11}$	$(4.2 \pm 0.3) \times 10^{-13}$	This work
4	$(1.3–3.2) \times 10^{15}$	$(2.3–13) \times 10^{14}$	3.2×10^{18}	0.5–2	$(1.3–4.8) \times 10^{11}$	$(1.1–9.6) \times 10^{11}$	$(4.2 \pm 0.2) \times 10^{-13}$	This work

a) Experimental conditions: The initial concentrations of reactants are described.

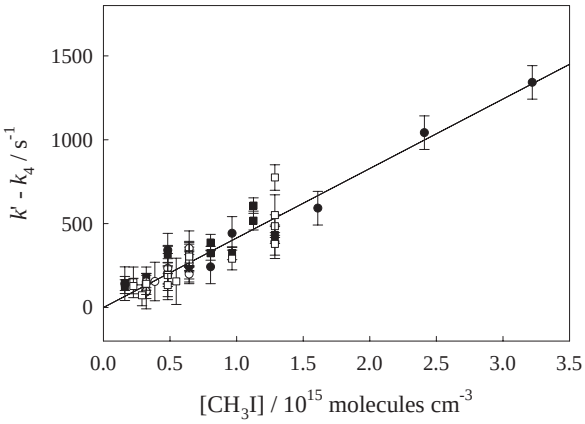

Figure 2. Second-order plots for $NO_3 + CH_3I$ in 100 Torr of total pressure at 298 K. The data are obtained under the several experimental conditions shown in Table 2. The data under the condition Nos. 1, 2, 3, and 4 are denoted by close circles, close squares, opened circles, and opened squares, respectively. The solid line is a linear least-squares fit to all data.

and the rate constants of reactions 15 and 16 ($k_{15} = 3.5 \times 10^{-11}$ cm^3 molecule^{-1} s^{-1} and $k_{16} = 1.0 \times 10^{-10}$ cm^3 molecule^{-1} s^{-1}), the pseudo-first-order lifetime for loss of NO_3 radicals by CH_3 radicals and I atoms could be estimated to be 45 and 16 ms, respectively. Because these lifetimes are much longer than the observed NO_3 decay profile of which example is shown in Figure 1, reactions 15 and 16 are considered to have no influence on the loss of NO_3 radicals. Thus, the decay profile of NO_3 measured in the presence of CH_3I could be analyzed by a single-exponential decay curve which is expressed by eqs 12 and 17.

$$k' = k_1[CH_3I] + k_4 \quad (17)$$

The value of k_4 gradually increased over a day by about a factor of two ($k_4 = 400–900\ s^{-1}$). It may be due to the effects by the products depositing on the wall of reaction cell. We measured k_4 in the absence of CH_3I before and after the measurements in the presence of CH_3I and corrected the change of k_4 in determining the rate constant of the reaction $NO_3 + CH_3I$. By this procedure, the pseudo-first-order rate constant for the loss of NO_3 via reaction $NO_3 + CH_3I$ could be extracted with reasonable accuracy. The plots described by open squares in Figure 2 shows $(k' - k_4)$ vs. $[CH_3I]$ measured under this condition. By a linear least-squares analysis, the rate constant of the reaction of $NO_3 + CH_3I$ was determined to be $k_1 = (4.2 \pm 0.3) \times 10^{-13}$ cm^3 molecule^{-1} s^{-1} at 298 K. Uncertainties reported herein are one standard deviation.

To completely check the influences of the sub-reactions such as reactions 15 and 16 on the determination of the rate constant of $NO_3 + CH_3I$, we consider all possible reactions as shown in Table 1. For CH_3 radicals and I atoms, reactions 18–21 in Table 1 should occur.[23,28–30] $O(^3P)$ atoms from reaction 3 react with CH_3I via reactions 22a–22f in Table 1. The branching ratios of reactions 22a, 22b, 22c, 22d, and 22f at 100 Torr with N_2 diluent are 0.44, 0.16, 0.07, <0.03, and <0.05, respectively.[31] Among these reaction products of reactions 22a–22f, CH_3 radical which is generated from the reac-

tion 22a, I atom from reactions 22c and 22d and OH radical from reaction 22b, possibly influence the loss of NO_3 by reactions 15, 16, and 23, respectively.

$$NO_3 + OH \rightarrow HO_2 + NO_2 \quad (23)$$

The rate constant of reaction 23 was reported to be 2.0×10^{-11} cm^3 molecule^{-1} s^{-1} at 298 K.[13] To estimate the influence of reactions 15, 16, and 23 on the loss of NO_3, temporal decay profiles of species in the reaction system were simulated with the IBM Chemical Kinetics Simulator Program using reactions 1, 4–11, 15, 16, and 18–23. Based on our simulation, NO_3 was predominantly consumed by reactions 1 and 4. The loss of NO_3 via reactions 15 and 16 under the initial conditions ($[CH_3]_0 = [I]_0 \leqq 6.3 \times 10^{11}$ molecules cm^{-3}) was estimated to be <2% and <5%, respectively. Other reactions had much smaller influence on the decay profile of NO_3. When reaction 4 was removed from the simulation, the loss of NO_3 via reactions 1, 15, and 16 were estimated to be >86%, <4%, and <9%, respectively. And also other reactions have much smaller influence. The loss of CH_3I by the reaction with NO_3 and $O(^3P)$ were estimated to be 0.02% and 0.01%, respectively. This indicates that the concentration of CH_3I was almost kept constant during the reaction measurement.

To suppress the influence of the reaction of $NO_3 + CH_3$, reaction 15, on the loss mechanism of NO_3, measurements with addition of 10 Torr of O_2 were carried out. CH_3 radicals were converted to CH_3O_2 by addition of O_2.

$$CH_3 + O_2 + M \rightarrow CH_3O_2 + M \quad (24)$$

The reported rate constant of reaction 24 at 298 K in 100 Torr of N_2 diluent was $k_{24} = 1.4 \times 10^{-12}$ cm^3 molecule^{-1} s^{-1}.[13] Based on the rate constant and the oxygen pressure used, O_2 scavenged CH_3 within 2 μs after the photolysis laser pulse. The following reaction of $NO_3 + CH_3O_2$ might occur.

$$NO_3 + CH_3O_2 \rightarrow NO_2 + CH_3O + O_2 \quad (25)$$

The reported rate constant of reaction 25 was $k_{25} = 1.3 \times 10^{-12}$ cm^3 molecule^{-1} s^{-1}.[13] Because almost all CH_3 radicals were converted to CH_3O_2 and the rate constant of the reaction of $NO_3 + CH_3O_2$ was much smaller than that of $NO_3 + CH_3$, the influence of the reactions 15 and 25 on the loss of NO_3 becomes smaller under these experimental conditions.

To determine the rate constant of NO_3 with CH_3I at 298 K in 100 Torr of total pressure, temporal profiles of $[NO_3]$ were measured with $(0.1–1.3) \times 10^{15}$ molecules cm^{-3} of CH_3I in the presence of 10 Torr of O_2. A typical example of the temporal profile of NO_3 in the presence of CH_3I is shown in Figure 1 with a best-fit curve using eq 12. As a result, the rate constant of reaction 1 in 100 Torr of ($N_2/O_2 = 9/1$) was determined to be $k_1 = (4.2 \pm 0.2) \times 10^{-13}$ cm^3 molecule^{-1} s^{-1}. This value is in good agreement with the rate constant determined above for 100 Torr of N_2 diluent without O_2.

Figure 2 is the second-order plots for $NO_3 + CH_3I$ in 100 Torr of total pressure at 298 K, including all data obtained in our previous and present study with and without O_2. By a linear least-squares analysis for these data, the rate constant at 298 K of the reaction of NO_3 radicals with CH_3I was determined to be $k_1 = (4.1 \pm 0.2) \times 10^{-13}$ cm^3 molecule^{-1} s^{-1}. The rate constants of reaction of NO_3 with CH_3I determined in this

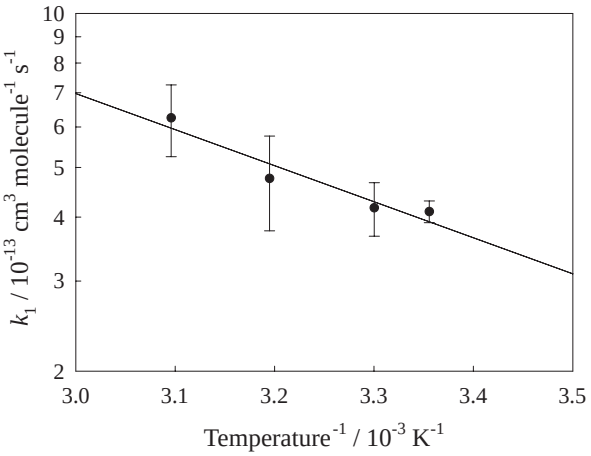

Figure 3. Temperature dependence of the rate constants for $NO_3 + CH_3I$ at 100 Torr of N_2 and O_2 diluent ($N_2/O_2 = 9/1$). The solid line is the linear least-squares fit.

and previous work under several different experimental conditions are summarized in Table 2. The values of rate constant of the reaction of NO_3 radicals with CH_3I were determined with several initial concentrations of NO_3, O_2, I, and CH_3. Especially for I and CH_3, even these initial concentrations changed by about 1/100 times, almost the same value of rate constant of the reaction of $NO_3 + CH_3I$ was obtained. And also experiments were performed with different concentration of N_2O_5 and photolysis laser power. These results show that the same values of the rate constant of the reaction of $NO_3 + CH_3I$ were obtained under different experimental conditions. Consequently, the results in Table 2 strongly suggest that the reactions of NO_3 with I atom and CH_3 radicals have no influence on the determination of the rate constant of the reaction of NO_3 radicals with CH_3I.

To determine the temperature dependence in 90 Torr of N_2 and 10 Torr of O_2 diluent, k_1 was measured at various temperatures, 298–323 K. Consequently, we obtain $k_1 = (4.2 \pm 0.6) \times 10^{-13}$ at 303 K, $(4.8 \pm 1.0) \times 10^{-13}$ at 313 K, $(6.3 \pm 1.0) \times 10^{-13}$ at 323 K, respectively. Figure 3 shows the Arrhenius plot of these data and indicates the positive temperature dependence for the reaction of $NO_3 + CH_3I$. A linear least-squares analysis of the data gives $k_1 = (9.1^{+18.4}_{-6.1}) \times 10^{-11} \exp[(-1600 \pm 300)/T]$ cm^3 molecule^{-1} s^{-1}. The activation energy was determined to be $E_a = 13 \pm 3$ kJ mol^{-1}.

As discussed in our previous paper,[10] the products are HNO_3 and CH_2I because only the following reaction pathway is exothermic.

$$NO_3 + CH_3I \rightarrow HNO_3 + CH_2I \quad (1)$$
$$\Delta_r H_{298} = -3.4 \pm 8.1 \text{ kJ mol}^{-1}$$

Here, $\Delta_r H_{298}$ was determined from the reported values of heats of formation of NO_3 ($\Delta_f H_{298} = 73.7 \pm 1.4$ kJ mol^{-1}),[13,32,33] CH_3I ($\Delta_f H_{298} = 13.76 \pm 0.12$ kJ mol^{-1}),[34] HNO_3 ($\Delta_f H_{298} = -134.3 \pm 0.5$ kJ mol^{-1}),[35] and CH_2I ($\Delta_f H_{298} = 218 \pm 8$ kJ mol^{-1})[36] at 298 K.

Discussion

Theoretical Study of the Reaction Mechanism. Optimized geometries of NO_3, CH_3I, HNO_3, and CH_2I are shown

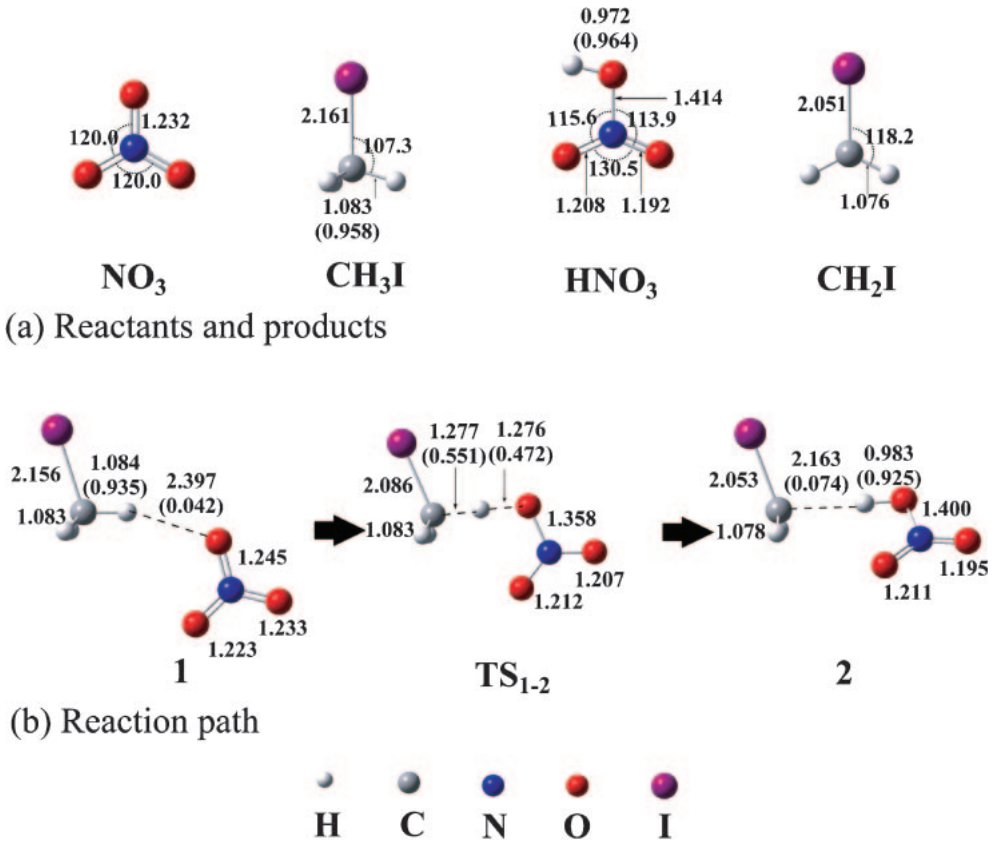

Figure 4. (a) Optimized structures of reactants and products and (b) geometrical change by H abstraction reaction. Bond lengths and angles are in Å and degrees, respectively. The values in parenthesis are Mayer's bond orders calculated at the B3LYP level.

in Figure 4a. Numerous theoretical and experimental studies of NO_3 reported that NO_3 takes D_{3h} geometry in the ground state.[37–42] In our calculation at the B3LYP level, the optimized geometry was in D_{3h} symmetry, as reported previously.[38] The optimized N–O bond length was 1.232 Å, which agreed well with MR-SDCI-calculated value reported by Eisfeld and Morokuma[39] (between 1.244 and 1.246 Å) and the experimental value (1.240 Å).[42]

Geometry changes by the H-abstraction reaction are summarized in Figure 4b, with Mayer's bond orders evaluated at the B3LYP level.[43,44] Complex **1** was formed by the interaction between the hydrogen of CH_3I and the oxygen of NO_3. The bond order of H–(CH_2I) was moderately smaller than in free CH_3I; 0.935 for complex **1** and 0.958 for free CH_3I. The bond order of H–O(NO_2) in complex **1** was 0.042. These results mean that the weak bond H–O(NO_2) is formed and the H–(CH_2I) bond is slightly weakened. One of the N–O bonds in NO_3 was slightly elongated; 1.232 Å for free NO_3 and 1.245 Å. In $\mathbf{TS_{1-2}}$, the hydrogen atom was located at nearly middle position between the carbon atom of CH_3I and the oxygen atom of NO_3 and the O–H–C moiety was nearly collinear. The bond orders of (CH_2I)–H and H–O(NO_2) were 0.551 and 0.472, respectively. Thus, the hydrogen atom interacts almost equally with both the carbon and the oxygen atoms, which is consistent with the geometry of $\mathbf{TS_{1-2}}$. After $\mathbf{TS_{1-2}}$, NO_3 abstracted a hydrogen atom, and a product complex (denoted **2**) composed of HNO_3 and CH_2I was formed. Actually, in complex **2**, the bond order of H–O(NO_2) was 0.925, which was close to that of free HNO_3 (0.964). A weak bonding interaction between CH_2I and HNO_3 was observed; the bond order was 0.074. It must be noted that we also found another reaction path, in which one oxygen of NO_3 interacted with the iodine of CH_3I through the reaction. However, it needed slightly higher activation barrier. Details appear in Supporting Information.

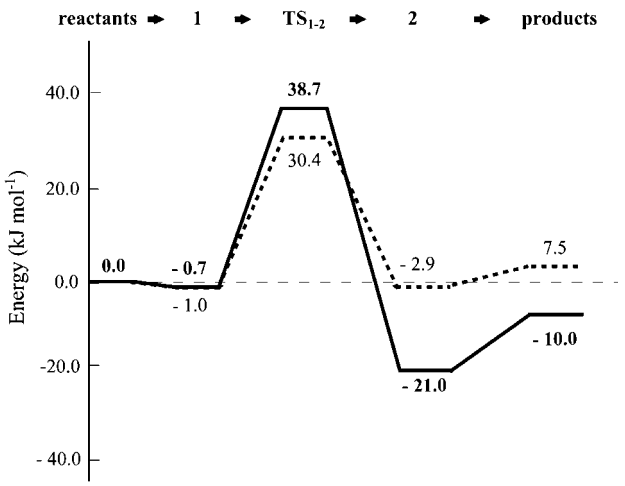

Figure 5. Potential energy diagram for $NO_3 + CH_3I \rightarrow HNO_3 + CH_2I$ calculated at the CCSD(T) (solid line) and B3LYP (dotted line) levels. The correction of zero-point energy was made (in kJ mol^{-1}).

Energy changes for the reaction are summarized in Figure 5, in which the sum of reactants was taken to be standard (energy zero) and the correction of zero-point energy was

Table 3. Three Model Runs to Test the Impact of the $NO_3 + CH_3I$ Reaction

	Rate constant /cm^3 molecule^{-1} s^{-1}	CH_3I flux from ocean diurnally constant /molecules cm^{-2} s^{-1}
Base run	0	1.5×10^7
Run A	$9.1 \times 10^{-11} \exp(-1600/T)$[a)]	1.5×10^7
Run B	$9.1 \times 10^{-11} \exp(-1600/T)$[a)]	6.0×10^7

a) Determined in this work

made in all these energies. Firstly, NO_3 attacked CH_3I, and a weakly bound complex **1** was formed. The stabilization energy calculated by the B3LYP method (1.0 kJ mol^{-1}) was almost the same as that by the CCSD(T) method (0.71 kJ mol^{-1}). The activation barrier was calculated to be 30.4 and 38.7 kJ mol^{-1} with the B3LYP and CCSD(T) methods, respectively. The CCSD(T)-calculated activation barrier was slightly higher than the B3LYP-calculated one. However, when $\mathbf{TS_{1-2}}$ was optimized with the BH&HLYP method, the CCSD(T)// BH&HLYP method presented a moderately smaller value (28.9 kJ mol^{-1}).[45] The relative energies of complex **2** were calculated to be -2.9 and -21.0 kJ mol^{-1} for B3LYP and CCSD(T), respectively. All the calculated activation barriers and reaction enthalpies $\Delta_r H$ were summarized in Table S1. Though the B3LYP-calculated ΔH_r of the reaction was positive (7.36 kJ mol^{-1}), the CCSD(T)-calculated ΔH_r values were negative (-4.35 to -19.66 kJ mol^{-1}). Thus, our CCSD(T) calculations reproduced the moderate exothermicity of the reaction. The $\Delta_r H_{298}$ value calculated from the reported $\Delta_f H_{298}$ value is -3.4 ± 8.1 kJ mol^{-1} as described above.

Atmospheric Model Calculations to Estimate the Importance of the Present Reaction in Atmospheric Chemistry. To test the impact of the $NO_3 + CH_3I$ reaction on atmospheric chemistry, three model runs were performed using a zero-dimensional box model with the conditions of 25 °C and 80% relative humidity, representing clean marine boundary layer. The background concentrations of atmospheric trace gases (NO_x, O_3, etc.) are similar to those used in the model runs for clean marine conditions in Morita et al.[46] Differences among the three runs are summarized in Table 3. In the base run, the $NO_3 + CH_3I$ reaction does not take place, whereas it occurs in the other two runs with the rate constant determined in the present work. The chemical reaction mechanism used in our model calculations is based on Regional Atmospheric Chemistry Mechanism reported by Stockwell et al.,[47] but is extended to include iodine chemistry (Supplement Table S3). Although inconsistency is found in the laboratory studies, the $OH + CH_3I$ and the $NO_3 + CH_3I$ reactions are assumed to produce CH_2IO_2 radicals in all the runs above. All the inorganic iodine species are assumed to undergo heterogeneous reactions on the surfaces of sea-salt particles with uptake coefficients of 0.5. Upon heterogeneous reactions of OIO, I_2O_2, and $IONO_2$, only half of the iodine atoms are recycled back to the gas phase, to represent the enrichment of iodine in the aerosol phase that is usually observed in the marine boundary layer.

For simplicity, the CH_3I fluxes from the ocean to the atmosphere are assumed to have no diurnal variations. In the base run and run B, the fluxes of CH_3I from the ocean to the atmosphere are assumed so that its diurnally averaged concentration in the atmosphere falls in the range of (3–4) $\times 10^7$ cm^{-3}, usually found in the clean marine boundary layer. The boundary layer height is assumed to be 1000 m. The entrainment velocity of the CH_3I-free air from the layer above the boundary layer is assumed to be 0.2 cm s^{-1}. All the inorganic iodine species are assumed to have dry deposition velocities of 0.5 cm s^{-1} on the ocean surface. The model runs are performed for 10-day long. The diurnal pattern of the last day is used as output. The results of the three model runs are summarized in Figure 6. Three main features are found:

(1) Effect of the $NO_3 + CH_3I$ reaction on the CH_3I levels and diurnal patterns (Figure 6a).

(2) Effect of the $NO_3 + CH_3I$ reaction on the NO_3 loss (Figure 6b).

(3) Activation of the inorganic iodine chemistry (Figures 6c and 6d).

For feature (1), the diurnally averaged CH_3I concentration level in the base run (4.4×10^7 cm^{-3} or 1.7 pptv) decreased to 7.4×10^6 cm^{-3} or 0.3 pptv) in run A by assuming the $CH_3I + NO_3$ reaction rate constant determined in the present work, suggesting the potential importance of the reaction in the CH_3I budget. The CH_3I flux needs to be increased by a factor of 4 so that the original level of CH_3I, usually found in the clean marine boundary layer, is reproduced in run B with the rate constant determined in the present work. The global emission rate of CH_3I needs to be increased by the similar factor, if calculated on the basis of atmospheric CH_3I burdens and its previously known loss chemistry (OH reaction and photolysis) in the atmosphere.

The diurnal pattern of the CH_3I concentration with a morning maximum and an evening minimum in the base run completely reverses to that with a morning minimum and an evening maximum in runs A and B, where the nighttime loss of CH_3I becomes dominant. If the diurnal pattern of CH_3I predicted in runs A and B is found in the atmosphere, it could be a strong evidence of the importance of the $NO_3 + CH_3I$ reaction. Oram and Penkett[48] measured the CH_3I concentration over open oceans at a ground-based at West Beckham in eastern England on summer in 1989 and September 1990. The observed diurnal pattern of the CH_3I concentration showed a morning minimum and an evening maximum. This observation is consistent with the predicted diurnal pattern of CH_3I by the present model calculation which includes the reaction of $NO_3 + CH_3I$. Thus, the atmospheric lifetime of CH_3I is significantly shortened by the reaction with NO_3. The role of CH_3I to carry the iodine atoms to high altitudes (including stratosphere) by convections in the tropics might not be significant as is currently thought.

For feature (2), the NO_3 levels in runs A and B are lower than the NO_3 level in the base run, suggesting the importance of CH_3I on the budget of NO_3.

For feature (3), the IO and I_x (total inorganic iodine, $[I_x] = [I] + [IO] + [HI] + [HOI] + [OIO] + 2[I_2O_2] + [INO] + [INO_2] + [IONO_2] + [IBr]$) levels in runs A and B increased in comparison to the base run especially during nighttime, suggesting the importance of the $NO_3 + CH_3I$ reactions to produce inorganic iodine species in the background marine atmosphere. Even during the daytime, the IO and I_x levels in runs A

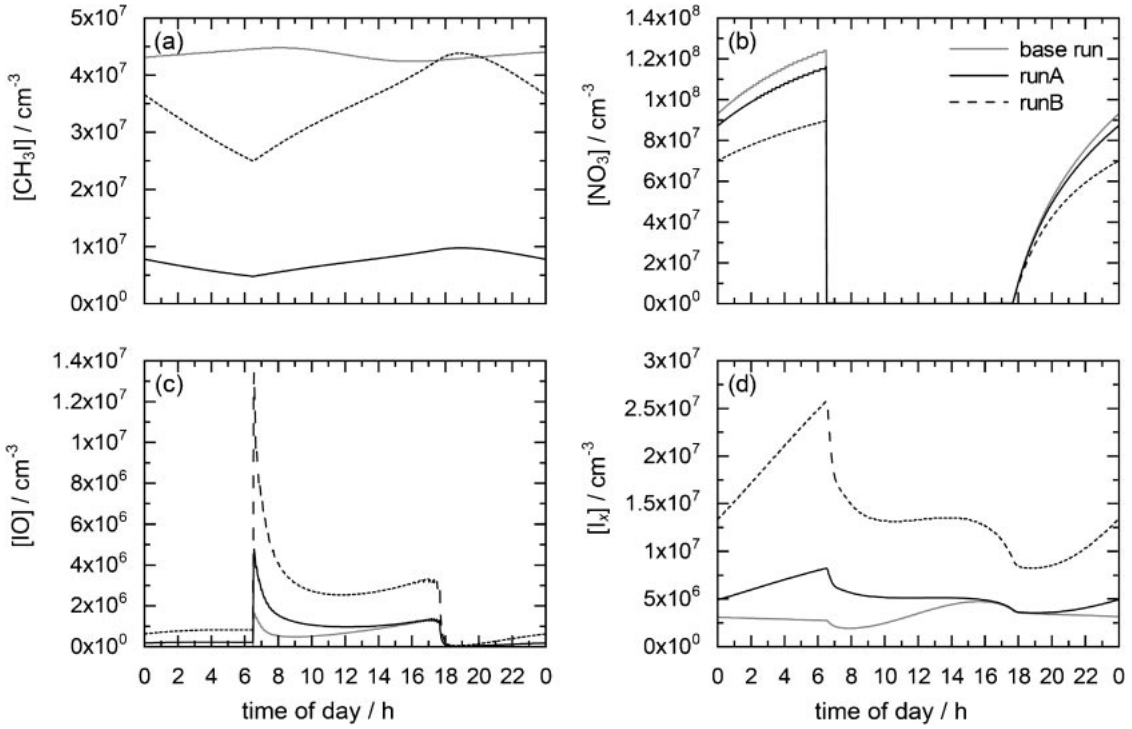

Figure 6. Diurnal variations of (a) CH_3I, (b) NO_3, (c) IO, and (d) total inorganic iodine (I_x) as calculated by three box model runs. See Supplement Table S3 for details of the runs.

and B are higher than those in the base run. It is likely that the inorganic iodine species produced during nighttime are still present in the atmosphere in the following daytime. The IO and I_x levels calculated in run B could be ubiquitous over the open oceans.

Although not shown, another model run was made assuming the production of HCOH and IO instead of CH_2IO_2 from the $OH + CH_3I$ and $NO_3 + CH_3I$ reactions, as suggested by Enami et al.[49] However, this run only resulted in similar levels of IO and I_x as those in run B.

The authors thank Prof. S. Aloisio of California State University (Channel Islands), Dr. S. Hashimoto and Dr. S. Enami of Kyoto University for their valuable discussions. This work was supported by the Global Environment Research Fund (RF-071) of the Ministry of the Environment, Japan. Y.N. is grateful to a Grant-in-Aid from the Ministry of Education, Culture, Sports, Science and Technology of Japan (No. 18710012) and grant from Mitsubishi Chemical Corporation Fund. Y.N. and T.I. are also grateful to a grant from Hiroshima City University for Special Academic Research (General Studies). M. K. thanks the Yazaki Memorial Foundation for financial support.

Supporting Information

Tables of all the calculated activation energies and reaction enthalpies. Cartesian coordinates of all the complexes and the transition states. Figures of geometry changes and energy changes by the reaction. The chemical reaction mechanism used in our model calculations is based on Regional Atmospheric Chemistry Mechanism reported by Stockwell et al.,[47] but is extended to include the iodine chemistry. This material is available free of charge on the web at http://www.csj.jp/journals/bcsj/.

References

1 A. Saiz-Lopez, J. M. C. Plane, *Geophys. Res. Lett.* **2004**, *31*, L04112.

2 B. Alicke, K. Hebestreit, J. Stutz, U. Platt, *Nature* **1999**, *397*, 572.

3 B. J. Allan, J. G. McFiggans, J. M. C. Plane, H. Coe, *J. Geophys. Res., [Atmos.]* **2000**, *105*, 14363.

4 D. Davis, J. Crawford, S. Liu, S. McKeen, A. Bandy, D. Thornton, F. Rowland, D. Blake, *J. Geophys. Res., [Atmos.]* **1996**, *101*, 2135.

5 G. McFiggans, J. M. C. Plane, B. J. Allan, L. J. Carpenter, H. Coe, C. O'Dowd, *J. Geophys. Res., [Atmos.]* **2000**, *105*, 14371.

6 J. M. Cronkhite, R. E. Stickel, J. M. Nicovich, P. H. Wine, *J. Phys. Chem. A* **1999**, *103*, 3228.

7 C. D. O'Dowd, J. L. Jimenez, R. Bahreini, R. C. Flagan, J. H. Seinfeld, K. Hämeri, L. Pirjola, M. Kulmala, S. G. Jennings, T. Hoffmann, *Nature* **2002**, *417*, 632.

8 J. L. Jimenez, R. Bahreini, D. R. Cocker, H. Zhuang, V. Varutbangkul, R. C. Flagan, J. H. Seinfeld, C. D. O'Dowd, T. Hoffmann, *J. Geophys. Res., [Atmos.]* **2003**, *108*, 4318.

9 C. E. Kolb, *Nature* **2002**, *417*, 597.

10 Y. Nakano, T. Ishiwata, M. Kawasaki, *J. Phys. Chem. A* **2005**, *109*, 6527.

11 Y. Ninomiya, S. Hashimoto, M. Kawasaki, T. J. Wallington, *Int. J. Chem. Kinet.* **2000**, *32*, 125.

12 Y. Nakano, T. Ishiwata, S. Aloisio, M. Kawasaki, *J. Phys. Chem. A* **2006**, *110*, 7401.

13 S. P. Sander, A. R. Ravishankara, D. M. Golden, C. E. Kolb, M. J. Kurylo, M. J. Molina, G. K. Moortgat, B. J. Finlayson-Pitts, P. Wine, R. E. Huie, *Chemical Kinetics and Photochemical Data for Use in Stratospheric Modeling: Evalua-*

tion 16, Jet Propulsion Laboratory, Pasadena, California, **2006**.
14 S. P. Sander, *J. Phys. Chem.* **1986**, *90*, 4135.
15 R. J. Yokelson, J. B. Burkholder, R. W. Fox, R. K. Talukdar, A. R. Ravishankara, *J. Phys. Chem.* **1994**, *98*, 13144.
16 G. V. Caesar, M. Goldfrank, *J. Am. Chem. Soc.* **1946**, *68*, 372.
17 A. D. Becke, *J. Chem. Phys.* **1986**, *84*, 4524.
18 C. Lee, W. Yang, R. G. Parr, *Phys. Rev. B* **1988**, *37*, 785.
19 T. H. Dunning, Jr., *J. Chem. Phys.* **1989**, *90*, 1007.
20 J. M. L. Martin, A. Sundermann, *J. Chem. Phys.* **2001**, *114*, 3408.
21 M. J. Frisch, G. W. Trucks, H. B. Schlegel, G. E. Scuseria, M. A. Robb, J. R. Cheeseman, J. A. Montgomery, Jr., T. Vreven, K. N. Kudin, J. C. Burant, J. M. Millam, S. S. Iyengar, J. Tomasi, V. Barone, B. Mennucci, M. Cossi, G. Scalmani, N. Rega, G. A. Petersson, H. Nakatsuji, M. Hada, M. Ehara, K. Toyota, R. Fukuda, J. Hasegawa, M. Ishida, T. Nakajima, Y. Honda, O. Kitao, H. Nakai, M. Klene, X. Li, J. E. Knox, H. P. Hratchian, J. B. Cross, C. Adamo, J. Jaramillo, R. Gomperts, R. E. Stratmann, O. Yazyev, A. J. Austin, R. Cammi, C. Pomelli, J. W. Ochterski, P. Y. Ayala, K. Morokuma, G. A. Voth, P. Salvador, J. J. Dannenberg, V. G. Zakrzewski, S. Dapprich, A. D. Daniels, M. C. Strain, O. Farkas, D. K. Malick, A. D. Rabuck, K. Raghavachari, J. B. Foresman, J. V. Ortiz, Q. Cui, A. G. Baboul, S. Clifford, J. Cioslowski, B. B. Stefanov, G. Liu, A. Liashenko, P. Piskorz, I. Komaromi, R. L. Martin, D. J. Fox, T. Keith, M. A. Al-Laham, C. Y. Peng, A. Nanayakkara, M. Challacombe, M. W. Gill, B. Johnson, W. Chen, M. W. Wong, C. Gonzalez, J. A. Pople, *Gaussian 03, Revision C.02*, Gaussian, Inc., Pittsburgh PA, **2003**.
22 A. R. Ravishankara, P. H. Wine, C. A. Smith, P. E. Barbone, A. Torabi, *J. Geophys. Res., [Atmos.]* **1986**, *91*, 5355.
23 R. Atkinson, D. L. Baulch, R. A. Cox, J. N. Crowley, R. F. Hampson, Jr., R. G. Hynes, M. E. Jenkin, J. A. Kerr, M. J. Rossi, J. Troe, *IUPAC Summary of Evaluated Kinetic and Photochemical Data for Atmospheric Chemistry*, **2006**.
24 P. Biggs, C. E. Canosa-Mas, P. S. Monks, R. P. Wayne, T. Benter, R. N. Schindler, *Int. J. Chem. Kinet.* **1993**, *25*, 805.
25 P. Biggs, C. E. Canosa-Mas, J. M. Fracheboud, D. E. Shallcross, R. P. Wayne, *J. Chem. Soc., Faraday Trans.* **1994**, *90*, 1197.
26 R. M. Chambers, A. C. Heard, R. P. Wayne, *J. Phys. Chem.* **1992**, *96*, 3321.
27 T. J. Dillon, M. E. Tucceri, R. Sander, J. N. Crowley, *Phys. Chem. Chem. Phys.* **2008**, *10*, 1540.
28 T. F. Hunter, K. S. Kristjansson, *J. Chem. Soc., Faraday Trans. 2* **1982**, *78*, 2067.
29 J. Albaladejo, E. Jimenez, A. Notario, B. Cabanas, E. Martinez, *J. Phys. Chem. A* **2002**, *106*, 2512.
30 K. H. Stephan, F. J. Comes, *Chem. Phys. Lett.* **1979**, *65*, 251.
31 M. K. Gilles, A. A. Turnipseed, R. K. Talukdar, Y. Rudich, P. W. Villalta, L. G. Huey, J. B. Burkholder, A. R. Ravishankara, *J. Phys. Chem.* **1996**, *100*, 14005.
32 S. Abramowitz, M. W. Chase, *Pure Appl. Chem.* **1991**, *63*, 1449.
33 H. F. Davis, B. Kim, H. S. Johnston, Y. T. Lee, *J. Phys. Chem.* **1993**, *97*, 2172.
34 S. A. Kudchadker, A. P. Kudchadker, *J. Phys. Chem. Ref. Data* **1975**, *4*, 457.
35 O. Dorofeeva, V. S. Iorish, V. P. Novikov, D. B. Neumann, *J. Phys. Chem. Ref. Data* **2003**, *32*, 879.
36 W. B. DeMore, S. P. Sander, D. M. Golden, R. F. Hampson, M. J. Kurylo, C. J. Howard, A. R. Ravishankara, C. E. Kolb, M. J. Molina, *Chemical Kinetics and Photochemical Data for Use in Stratospheric Modeling, Evaluation No. 10*, Jet Propulsion Laboratory, Pasadena, California, **1994**.
37 J. F. Olsen, L. Burnelle, *J. Am. Chem. Soc.* **1970**, *92*, 3659.
38 C. D. Sherrill, M. S. Lee, M. Head-Gordon, *Chem. Phys. Lett.* **1999**, *302*, 425.
39 W. Eisfeld, K. Morokuma, *J. Chem. Phys.* **2000**, *113*, 5587.
40 N. Mora-Diez, R. J. Boyd, *J. Phys. Chem. A* **2002**, *106*, 384.
41 T. Uchimaru, S. Tsuzuki, M. Sugie, K. Tokuhashi, A. Sekiya, *Chem. Phys.* **2006**, *324*, 465.
42 T. Ishiwata, I. Tanaka, K. Kawaguchi, E. Hirota, *J. Chem. Phys.* **1985**, *82*, 2196.
43 I. Mayer, *Chem. Phys. Lett.* **1985**, *117*, 396.
44 I. Mayer, *Program "BORDER," Version 1.0*, Chemical Research Center, Hungarian Academy of Sciences, Budapest, **2005**.
45 We also calculated the activation barrier by the CCSD(T)//BH&HLYP method, in which BH&HLYP geometries were used in the CCSD(T) calculations except for NO_3 for which the MP2 calculated-structure was used. The CCSD(T)//BH&HLYP procedure was introduced by Mora-Diez and Boyd and presented the reasonable result, in their study on the reaction of NO_3.[40] In our calculation, the calculated-activation barrier was 29.1 kJ mol^{-1}.
46 A. Morita, Y. Kanaya, J. S. Francisco, *J. Geophys. Res., [Atmos.]* **2004**, *109*, D09201.
47 W. R. Stockwell, F. Kirchner, M. Kuhn, S. Seefeld, *J. Geophys. Res., [Atmos.]* **1997**, *102*, 25847.
48 D. E. Oram, S. A. Penkett, *Atmos. Environ.* **1994**, *28*, 1159.
49 S. Enami, J. Ueda, M. Goto, Y. Nakano, S. Aloisio, S. Hashimoto, M. Kawasaki, *J. Phys. Chem. A* **2004**, *108*, 6347.